Catal Lett (2012) 142:1321–1329
DOI 10.1007/s10562-012-0906-1

Carbon Supported Pd Nanocrystals as High Efficient Catalyst for Regioselective Hydrogenation of *p*-Phenylphenol to *p*-Cyclohexylphenol

Chengyun Liu · Lianhai Lu · Zeming Rong · Changhai Liang · Yue Wang · Qingping Qu

Received: 19 December 2011 / Accepted: 11 September 2012 / Published online: 25 September 2012

Abstract A series of Pd based nanocrystals were used to catalyze regioselective hydrogenation of *p*-phenylphenol (*p*-PP) to *p*-cyclohexylphenol (*p*-CP). The polar solvents such as THF, methanol and ethanol offered much higher selectivity to *p*-CP than nonpolar solvent. Concerning the effect of supports, the active carbon supported Pd nanocrystals show the best performance probably due to its hydrophobicity and high surface area. The best result with high selectivity (89.1 %) was obtained by using Pd/active carbon as catalyst when *p*-PP was 100 % converted.

Keywords Regioselective hydrogenation · Support effect · Pd nanocrystal · *p*-Phenylphenol · *p*-Cyclohexylphenol

1 Introduction

p-Cyclohexylphenol (*p*-CP), a very important fine chemical, has been widely used in the production of antioxidants of elastomers, liquid crystal monomers, high pressure lubricates and automatic transmission fluids [1, 2]. Several methods such as the Friedel–Crafts alkylation of phenol with cyclohexanol or cyclohexene using acidic catalyst and the hydrogenation of *p*-phenylphenol (*p*-PP) have been most studied to produce *p*-CP [3, 4]. For the Friedel–Crafts alkylation, the major products were *o*-cyclohexylphenol, *p*-cyclohexylphenol, cyclohexyl phenyl ether and some polyalkylated phenols. However, the existence of hydroxyl group in phenol favors the formation of *o*-cyclohexylphenol (*o*-CP) and reduces the selectivity to *p*-CP in the product mixture. On the other hand, catalytic hydrogenation is a more environmentally benign approach that is a promising route to produce *p*-CP. Especially, the heterogeneous catalytic hydrogenations which the catalysts can be recyclable used have been extensively studied to hydrogenate bicyclic aromatics. Smith et al. [5] obtained essentially pure cyclohexylphenyl intermediates in the half-hydrogenation of diphenylmethane and 1, 1-diphenylethane. Similarly, a minimum of 90 % phenylcyclohexylacetic acid was formed from diphenylacetic acid over Adams platinum oxide. Gates and coworkers [6, 7] studied the hydrogenation kinetics of biphenyl over sulfided CoO-MoO_3/γ-Al_2O_3. Lu et al. [8] studied the selective hydrogenation of single benzene ring in biphenyl by using skeletal Ni and obtained the yield of 99.4 %. Furthermore, dilute aqueous alkaline solutions [9] and supercritical carbon dioxide [10] have also been used to investigate the selective hydrogenation of bicyclic aromatics. However, all the examples mentioned above are focused on the symmetric molecule, under controlled reaction condition; the reaction will get ideal selectivity to single ring hydrogenated products since the two phenyl groups are equal. For the hydrogenation of the asymmetric *p*-PP, there are very limited studies available, since the difference between phenyl group and phenol group make it difficult to get selectively hydrogenated products. Tsukinoki et al. [10] have used Raney Ni–Al alloy in dilute aqueous alkaline solution as the reaction system to produce *p*-CP with the yield of 30 %. Adkins and coworkers [11] studied the

Electronic supplementary material The online version of this article (doi:10.1007/s10562-012-0906-1) contains supplementary material, which is available to authorized users.

C. Liu · L. Lu · Z. Rong (✉) · C. Liang · Y. Wang · Q. Qu (✉)
State Key Laboratory of Fine Chemicals, Dalian University of Technology, Dalian 116024, China
e-mail: zeming@dlut.edu.cn

Q. Qu
e-mail: qujp@dlut.edu.cn

different hydrogenation processes of *p*-PP over Raney-Ni and copper–chromium oxide and obtained the selectivity to *p*-CP of 43 and 48 %, respectively. Minabe et al. [12] have studied the trends of selective hydrogenation of 4-subsituted biphenyl over Pd/AC, PtO_2 and Raney-Ni and pointed out that the effect of the position of the substituent is only observed in the reaction with Pd/C. But further investigations of hydrogenation behavior over Pd/AC were not carried out. Recently, our group has successfully developed a new catalytic system by using hydrazine-reduced Pd/AC as catalyst and THF as the reaction solvent [13]. Though the selectivity to *p*-CP is 92.3 %, the turnover frequency (TOF) is still not satisfactory for industrial application. Therefore, a more effective catalyst with higher activity and relatively high selectivity is required. In this paper, we report our recent discovery on the selective hydrogenation of *p*-PP to *p*-CP by using a carbon supported Pd nanocrystal catalyst. The effects of supports and Pd precursors were studied.

2 Experimental

2.1 Preparation of Catalyst

2.1.1 Materials

$PdCl_2$ and $Pd(OAc)_2$ with purity over 99.0 % were purchased from Heraeus company. Na_2PdCl_4 was prepared by the coordination between $PdCl_2$ and NaCl at a molar ratio of 1:2 under 343 K for 15 min. $PdCl_2(en)_2$ was synthesized by reacting a solution of Na_2PdCl_4 with certain drops of ethylenediamine. The multi-wall carbon nanotubes and graphite were pretreated by nitric acid at 80 °C for 1 h, after which they were washed by excess deionized water. All the other chemicals were purchased from Sinopharm Chemical Reagent Co., Ltd and were used as received without further processing or purification.

2.1.2 The Preparation of Pd Nanocrystal Catalysts

The carbon supported Pd nanocrysal catalysts were prepared by chemical reduction of Na_2PdCl_4, $Pd(OAc)_2$ and $PdCl_2(en)_2$ with $NaBH_4$ aqueous solution. The preparation procedure was typically as follows: certain amounts of Pd precursors (with 0.053 g Pd net weight) were quantitatively added to 50 ml solution, which was a mixture of deionized water and acetone (with the volume ratio of 1:1) containing both Tween-20 (polyethylene glycol sorbitan monolaurate, $C_{58}H_{113}O_{26}$) and Brij-35 (polyoxyethylenelauryl ether, $C_{12}H_{25}O(OCH_2CH_2)_{23}H$) with ten times CMC [14]. Then 1 g carbon supports were added into the system in order to adsorb the Pd species and keep stirring. After stirring 4 h, the carbon supports were filtrated from the system and keep in vacuum oven overnight at 110 °C to remove the adsorbed water. In order to maximally adsorb the Pd species, these carbon supports were added into the solution again and keep stirring for 4 h before the step of reduction. Then, 0.2 g $NaBH_4$ in 50 ml H_2O was dropwisely added to the solution within 30 min. After stirring for 2 h, the carbon supported Pd nanocrystal catalysts were recovered by centrifuging (under 3,000 r/min for 30 min), and washed with deionized water and alcohol. The prepared catalysts were kept in Schlenk flasks with N_2 protecting and the percolate was collected to detect the amounts of palladium and chlorine species by ICP and ion chromatography, respectively.

The TiO_2, SiO_2 and γ-Al_2O_3 supported Pd nanocrystal catalysts were prepared by using $Pd(OAc)_2$ as the precursor and the process is similar as described above.

2.2 Characterization of Pd Nanocrystal Catalysts

2.2.1 X-Ray Diffraction (XRD)

Diffraction profiles were determined at room temperature using a hybrid Hilton-Brooks generator fitted with a Cu Kα ($\lambda = 1.5406$ Å) X-ray source coupled to a Phillips diffract meter containing a scintillator detector. The samples were generally scanned over the range $2\theta = 10$–$80°$, typically using a step interval of 2°/min. Diffracted X-rays were collected using a real time multiple strip detector.

2.2.2 Transmission Electron Microscopy (TEM)

TEM analysis was performed using JEOL 2010F equipped with a Schottky field emission gun operated at 200 kV. Samples were prepared by grinding and suspending the Pd nanocrystal catalysts in ethanol, and then a small amount of this solution was dropped onto a carbon coated copper grid and allowed to dry before loading the sample in the TEM.

2.2.3 BET

Specific surface area measurements were obtained by volumetric nitrogen adsorption using a Micromeritics ASAP-2010 instrument. Measurements were obtained using 0.10 g of catalyst weighed into a sample tube and conditioned at 250 °C for 4 h and 5×10^{-5} Torr. Following out-gassing, the samples were cooled to ambient temperature prior to adsorption measurements. The analysis was carried out by dosing nitrogen at −196 °C, with the variation in pressure allowing the adsorbed volume of N_2 to be determined.

2.2.4 H_2-Temperature-Programmed Desorption (H_2-TPD)

H_2-TPD desorption of hydrogen experiments were performed by America Micromeritics Autochem 2720 equipment. First,

50 mg of the sample was reduced in a 10 % H_2/Ar gas mixture at 523 K (with the heating rate of 10 K/min) for 1 h under a flow rate of 50 mL/min. Once the catalysts were cooled down to room temperature, the surface was purged in an argon flow for 1 h. Then, the TPD were conducted in flowing Ar at 10 K/min to 825 K.

2.2.5 *Elemental Analysis (ICP-AES and Energy Dispersive Spectroscopy (EDS))*

The real percentage of Pd loading on different supports was detected by ICP-AES (Varian VISTA- MPX). Briefly, 0.1 g of each samples were dissolved in aqua regia and diluted into 1 mg/ml solution and then performed the ICP detection.

The amounts of chlorine anion on the surface of Pd/activated carbon were detected by the EDS which was recorded with a JEOL 7500F field emission scanning electron microscope. EDS line scan data were collected using an acceleration voltage of 200 kV with a 0.5 nm diameter probe. Integrated intensities obtained from the Pd *L* and Cl *K* lines were used for quantification of the two elements, respectively.

2.2.6 *Boehm Titration*

The quantity of the surface oxygen-containing groups for carbon supports were measured according to the method suggested by Boehm [15–17]. Generally, 0.25 g of each kind of carbon support was placed in a bottle, to which 25 ml of 0.1 N solution of Na_2CO_3, $NaHCO_3$ or NaOH was added, and the bottles were sealed. After shaking for 24 h, 20 ml of the solution were back-titrated using 0.05 N·HCl. The amounts of NaOH and $NaHCO_3$ reacted were used to calculate the total number of acidic groups (phenol, lactone, and carboxylic groups) and the number of carboxylic groups, respectively. Na_2CO_3 consumption indicated the amount of both lactone and carboxylic groups. Consequently, the number of lactone groups was determined from the difference in Na_2CO_3 and $NaHCO_3$ consumption. The number of phenol groups was determined from the difference between NaOH and Na_2CO_3 consumption. The overall quantity of basic groups was determined by titration with 0.1 N HCl and back-titrated with 0.05 N NaOH.

2.3 Hydrogenation Reaction

The hydrogenation reaction was carried out in a 70 mL stainless steel autoclave equipped with a magnetic stirrer. Catalysts were washed with deionized water and solvent five times before being added to the reactor. Then the *p*-PP, solvent and catalyst were quantitatively introduced to the reactor. The autoclave was sealed and purged with N_2 at least five times to expel air and then H_2 was introduced into the reactor to replace N_2. The reaction was started after the reaction temperature increased to the set point and the H_2 pressure was modified to the desired value.

The reaction process was monitored by taking small amounts of the reaction mixture at set time intervals. The samples were analyzed by GC (Agilent 6890, FID detector) with a 30 m HP-5 capillary column and PEG-20 M capillary column using a temperature ramp from 423 to 483 K at rate of 5 K/min. The calibrated area normalization method was used. The separations of different products were performed by using column chromatography on silica gel (*n*-hexane/EtOAc, 50:1) and the structural characteristics of products were accomplished by GC–MS (GCT CA156) and ^{1}H NMR (Varian INOVA). Details are described in the electronic supporting information (ESI).

3 Results and Discussion

3.1 Comparison of Different Catalytic Systems

The performance of six catalytic systems in the hydrogenation of *p*-PP is summarized in Table 1. Obviously, all the Pd-based catalysts exhibited higher selectivity to *p*-CP (over 75 %) while 5 wt% Pt/AC and 5 wt% Ru/AC preferred the deep hydrogenation of *p*-PP and Skeletal Ni slightly inclined to produce *p*-PC. The *trans*-/*cis*- ratios of *p*-PC and *p*-CC are dominated by the kind of metal used in the catalyst and, generally, the *cis*-configuration of *p*-PC and *trans*-configuration of *p*-CC are favored. Further compared the three kinds of 5 wt% Pd/AC, though the commercial 5 wt% Pd/AC (supported by Tongyong Chemicals Dalian, China) and the 5 wt% Pd/AC prepared according to the method mentioned in ref [12] resulted in acceptable selectivity to *p*-CP, however, the activity were much lower than the 5 wt% Pd/AC prepared in this paper. Therefore, take both the activity and selectivity into consideration; the Pd/AC catalyst prepared this time is the suitable catalyst for selective hydrogenation of *p*-PP to produce *p*-CP.

3.2 Effects of Solvents

The effects of different solvents are listed in Table 2. As shown, the selectivity to *p*-CP was over 70 % when using polar solvents as the reaction medium and the highest selectivity was obtained with THF. In contrast, when using cyclohexane as solvent, the selectivity to *p*-CP was only 12 % even though the highest activity was obtained in this condition. These results maybe caused by the different properties of solvents and the structural characteristic of

Table 1 Comparison of different catalytic systems

Entry	Catalysts	Conv. (%)	*p*-CP (%)	*p*-PC (*trans*-/*cis*-) (%)	*p*-CC (*trans*-/*cis*-) (%)
1	Skeletal Ni	36	46.0	53.4 (1/2.5)	0.4 (2.1/1)
2	5 wt% Pt/AC	23	51.5	29.2 (1/3.4)	19.3 (1.3/1)
3	5 wt% Ru/AC	72	38.2	22.1 (1/6.2)	39.2 (1.1/1)
4	5 wt% Pd/AC	29	87.0	12.7 (1/1.3)	0.3 (11/1)
5	5 wt% Pd/AC[a]	7	85.0	16.7 (1/1.3)	0.3 (11/1)
6	5 wt% Pd/AC[b]	5	78.0	21.8 (1/1.2)	0.2 (11/1)

Reaction conditions: *p*-PP 1.5 g, THF 20 mL, Cat. 0.5 g, 373 K, 2 MPa, 1 h

[a] 5 wt% Pd/AC prepared using the method reported by our group before in ref. [12]

[b] Commercial Pd/AC supported by Tongyong chemicals Dalian, China

Table 2 Effect of solvents in the hydrogenation of *p*-PP over Pd/AC

Entry	Solvents	Dielectric constant	Conv. (%)	*p*-CP (%)	*p*-PC (*trans*-/*cis*-) (%)	*p*-CC (*trans*-/*cis*-) (%)
1	ethanol	25.7	48	82	17.7 (1/1.3)	0.3 (10.1/1)
2	THF	7.58	29	87	12.7 (1/1.3)	0.3 (11/1)
3	isopropyl alcohol	18	37	76	13.4 (1/1.2)	0.6 (9.8/1)
4	ethyl acetate	6.02	36	78	21.5 (1/1.2)	0.5 (10.5/1)
5	cyclohexane	2.02	100	12	56.0 (1/1.1)	32.0 (8.8/1)

Reaction conditions: *p*-PP 1.5 g, solvent 20 mL, Pd/AC (prepared from $Pd(OAc)_2$) 0.5 g, 373 K, 2.0 MPa, 1 h

Table 3 Comparison of supported Pd nanocrystal catalysts

Entry	Catalysts	Surface area (m^2/g)	Pd loading (wt%)	TOF[a] (mol/g/h) × 10^{-2}	Conv. (%)	*p*-CP (%)	*p*-PC (*trans*-/*cis*-) (%)	*p*-CC (*trans*-/*cis*-) (%)
1	Pd/Al_2O_3	232	3.0	10.6	18	43	56.8 (1/1.3)	0.2 (10.9/1)
2	Pd/SiO_2	715	3.4	5.7	11	48	51.9 (1/1.3)	0.1 (11.2/1)
3	Pd/TiO_2	54	2.8	5.7	9	47	52.8 (1/1.3)	0.2 (12/1)
4	Pd/AC	1725	4.5	11.4	29	87	12.7 (1/1.3)	0.3 (11/1)
5	Pd/MWCNTs	55	2.3	16.1	21	59	40.2 (1/1.5)	0.8 (10.8/1)
6	Pd/graphite	6	1.7	5.2	5	53	46.7 (1/1.1)	0.3 (11/1)

Reaction conditions: *p*-PP 1.5 g, THF 20 mL, Cat. 0.5 g, 373 K, 2.0 MPa, 1 h

[a] TOF was calculated as the moles of *p*-PP consumed in 1 h divided by the total gram of metal inside the catalyst

p-PP. Generally, the solubility of hydrogen would be higher in the solvents with lower dielectric constant [18]. As shown in Table 2, the dielectric constant of cyclohexane is much lower than the other solvents and, consequently, the reaction would be accelerated by the high solubility of hydrogen. However, though the dielectric constants of ethanol and isopropyl alcohol are both higher than THF, the faster reaction speed would be explained by the high hydrogen donating abilities of these two solvents. On the other hand, when using the polar solvents as the reaction medium, the phenol part of *p*-PP inclined to be solvated into the solvent phase and led to the benzenoid ring of *p*-PP being more easily contacted with Pd nanocrystal which induced higher selectivity to *p*-CP. In contrast, when using cyclohexane (typical non-polar compound) as solvent, the benzenoid ring of *p*-PP preferred to be solvated which increased the reaction taking place at the phenol part of *p*-PP thus lowering the selectivity to *p*-CP. Therefore, taking both the selectivity and activity into account, THF is the proper solvent for this reaction.

3.3 Effect of Supports

The results of different supported Pd nanocrystal catalysts in the hydrogenation of *p*-PP are shown in Table 3. The active carbon supported Pd nanocrystal catalyst was found to have the highest activity and selectivity among the selected samples. As for the supported nanocrystal catalyst, the metal loading and the particle dispersion will strongly affect the catalytic performance. In Table 3, the AC hold

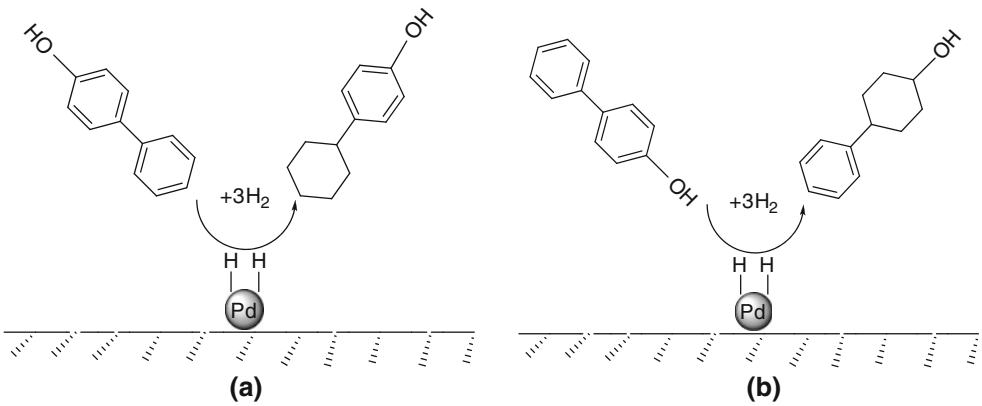

Scheme 1 Proposed adsorption modes of *p*-PP over different supports. **a** Adsorption of benzene ring in *p*-PP firstly and gives rise to *p*-CP. **b** Adsorption of phenol ring in *p*-PP firstly and gives rise to *p*-PC

Table 4 Boehm titration of carbon supports

Entry	Surface area (m^2/g)	Carboxyl groups (mmol/g) × 10^2	Lactone groups (mmol/g) × 10^2	Phenol groups (mmol/g) × 10^2	Basic groups (mmol/g) × 10^2	Total polar groups (mmol/g) × 10^2	Density of polar groups (mmol/m^2) × 10^4
Actived carbon	1725	7.5	1.3	31.3	50	90	5
MWCNTs	55	10	6.3	6	5	27.3	50
Graphite	6	7.5	3.8	1.2	7.5	20	333

Table 5 Effect of Pd/AC prepared from different Pd precursors

Precursor	Conv. (%)	*p*-CP (%)	Average particle size (nm)	Surface area (m^2/g)	Residual chlorine[a] (wt%)
$Pd(OAc)_2$	29	87	3.9	1830	0
$PdCl_2$	18	78	5.8	1700	0.3
$PdCl_2(en)_2$	8	62	16.6	1580	1.2

Reaction conditions: *p*-PP 1.5 g, THF 20 mL, Cat. 0.5 g, 1 h, 373 K, 2 MPa

[a] The amount of chlorine on the surface of catalysts was measured by EDS and shown in ESI

much larger specific surface area than the other supports which offered more sites to anchor Pd nanocrystals, and, consequently, the Pd loading on AC would be the largest among all selected samples. Also, the Pd nanocrystals dispersed on the surface of AC were evenly distributed within the range of 3–4 nm, however, on the surface of TiO_2, Al_2O_3, SiO_2 and graphite, the distribution of nanocrystals were broader and some aggregations were appeared (shown in ESI). But, surprisingly, though the surface area of MWCNTs is much lower than AC, the TOF value of Pd/MWCNTs is higher than Pd/AC. This phenomenon maybe caused by two reasons: the narrower distribution of Pd nanocrystals (seen in ESI) which caused by the pretreatment of MWCNTs and the well-known hydrogen storage properties of carbon nanotubes [19, 20].

From the aspect of selectivity, the carbon based catalysts clearly exhibited higher selectivity to *p*-CP than the other supported catalysts. Due to the polarity of phenol part and benzenoid part are different; the interaction of these two parts with catalyst surface will be the key factor to dominate the adsorption process of *p*-PP (shown in Scheme 1) and, consequently, the selectivity to *p*-CP. In the case of metal oxides supports, the interaction between the hydroxyl group of *p*-PP and the hydroxyl groups on the surface of metal oxides will increase the adsorption of phenol part and decrease the selectivity to *p*-CP. By contrast, in the case of carbon based catalysts, the hydrophobicity of carbon may favor the adsorption of benzenoid part to the surface of catalyst firstly and enhance the selectivity to *p*-CP [13, 21–23]. However, the inert surface of MWCNTs and graphite made it difficult to stabilize Pd nanocrystal, it is, hence, necessary to functionalize the surface of MWCNTs and graphite before stabilizing the Pd nanocrystals. But the introduced functional groups will also change the surface hydrophobicity and further change the adsorption process of *p*-PP [24]. The Boehm titration was performed to quantity investigates the surface condition of the used carbon supports (shown in Table 4). It could be found that though the AC support holds the largest number of polar groups the density of polar group, contrary, is

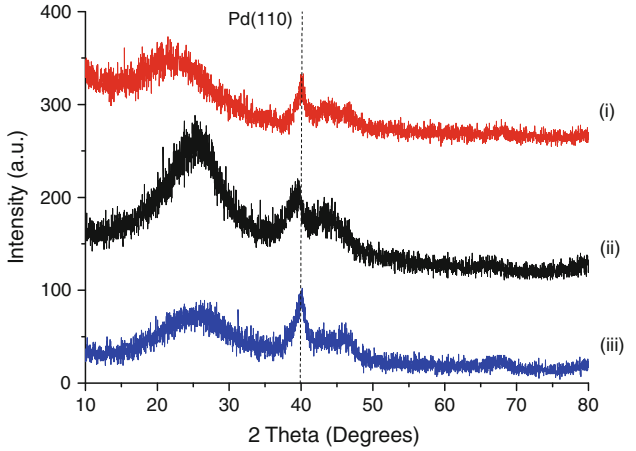

Fig. 1 XRD patterns of Pd nanocrystals prepared from different precursors *i* $PdCl_2$, *ii* $Pd(OAc)_2$, *iii* $PdCl_2(en)_2$

lowest among the carbon supports. Because the process of selective adsorption is a kind of microscale behavior, AC which holds the lowest density of polar groups would favors the adsorption benzenoid part of *p*-PP and further deduces the high selectivity to *p*-CP. Take both the activity and selectivity into account; the AC was the proper support for this reaction.

3.4 Effect of Pd Precursors

The effect on catalytic performance and the structure properties of Pd/AC prepared using different kinds of Pd precursors is shown in Table 5. It can be seen that for Pd/AC using $Pd(OAc)_2$ as precursor, the catalyst exhibited the highest activity and selectivity to *p*-CP. XRD patterns of these three kinds of Pd/AC are shown in Fig. 1. At around 40 ° (2θ), which corresponds to the diffraction of Pd(110) facet, the half-peak breadth of the peak derived from $Pd(OAc)_2$ is broader than the ones derived from $PdCl_2$ and $PdCl_2(en)_2$. This means the Pd nanocrystals synthesized from $Pd(OAc)_2$ were smaller than the ones prepared from $PdCl_2$ and $PdCl_2(en)_2$. TEM of these catalysts (Fig. 2) further informs us that the Pd nanocrystals synthesized from $Pd(OAc)_2$ are evenly distributed with the average diameter of 3.9 nm while the $PdCl_2$ and $PdCl_2(en)_2$ ones are distributed with the average diameter 5.8 and 16.4 nm, respectively. Because the catalytic activity of nanostructured catalysts strongly depends on its particle size, the high activity of Pd/AC prepared from $Pd(OAc)_2$ probably resulted from the relatively small diameter of Pd particles which hold much more exposed surface area. Also, it is well known that residual Cl^- can remain in the catalyst after pretreatment and significantly influences the properties of the catalyst [25–32]. From the results of EDS detection (in Table 5), the amount of residual Cl^- in the Pd/AC prepared by using $PdCl_2(en)_2$ as precursor was much higher than the one prepared by using $PdCl_2$ as precursor and these Cl^- could block some active sites on the surface of Pd and further reduce the catalytic activity. The TPD profiles of these catalysts are shown in Fig. 3 and there are three kinds of peaks could be found. The peaks exists at 373 and 463 K are corresponding to two kinds of Pd hydride: the α-phase Pd hydride which exists on the surface of Pd nanocrystal and the *β*-phase Pd hydride which dissolves in the lattice of Pd nanopartical and the peaks exists at 663 K are corresponding to the desorption of spillover-hydrogen [33]. Interestingly, in the case of $Pd(OAc)_2$, the peak of *β*-phase Pd hydride is much stronger than the peak of α-phase Pd hydride while in other cases, the peaks of α-phase Pd hydride are stronger than the peaks of *β*-phase Pd hydride, these differences maybe caused by the existence of Cl^- and ethanediamine on the surface of Pd nanocrystals which reduced the dissolving of hydrogen into the Pd lattice and further inhibited the formation of *β*-phase Pd hydride. Also, the strength of the peaks derived from $Pd(OAc)_2$ are much stronger than the ones derived from $PdCl_2$ and $PdCl_2(en)_2$ which indicates that the $Pd(OAc)_2$ one holds much more actived hydrogen and thus obtains the best activity, correspondingly. Moreover, the existence of Cl^- and ethanediamine such hydrophilic ligands could change hydrophobicity of carbon and thus affects the adsorption process which further decreases the selectivity to *p*-CP in this reaction. From both the activity and selectivity, the $Pd(OAc)_2$ could be the proper precursor to prepare Pd/AC.

3.5 Effects of Reaction Temperature and Pressure

In order to optimize the reaction conditions, effects of different parameters were investigated. Figure 4a (detail numbers were shown in ESI) shows the effect of reaction temperature under a constant reaction pressure 4.0 MPa. In the range of 353–383 K, the catalytic activity increased with the increase of reaction temperature, as expected. In addition, the selectivity reached the maximum of over 85 % at 363 K, before slightly decreasing with further increase of reaction temperature. Due to the surface hydrophobicity of AC, which favors the prior adsorption of benzene ring and induce the production of *p*-CP, proper temperature will increase the chance of interaction between *p*-PP and the surface of AC and thus enhance the selectivity to *p*-CP. But further increase the reaction temperature, the increased adsorption and desorption intensity will left less time for the prior regioselective adsorption of benzene ring part to the catalyst surface and reduce the corresponding reaction selectivity. Since selectivity is the most important factor to be taken into account, 363 K should be adopted as the proper reaction temperature.

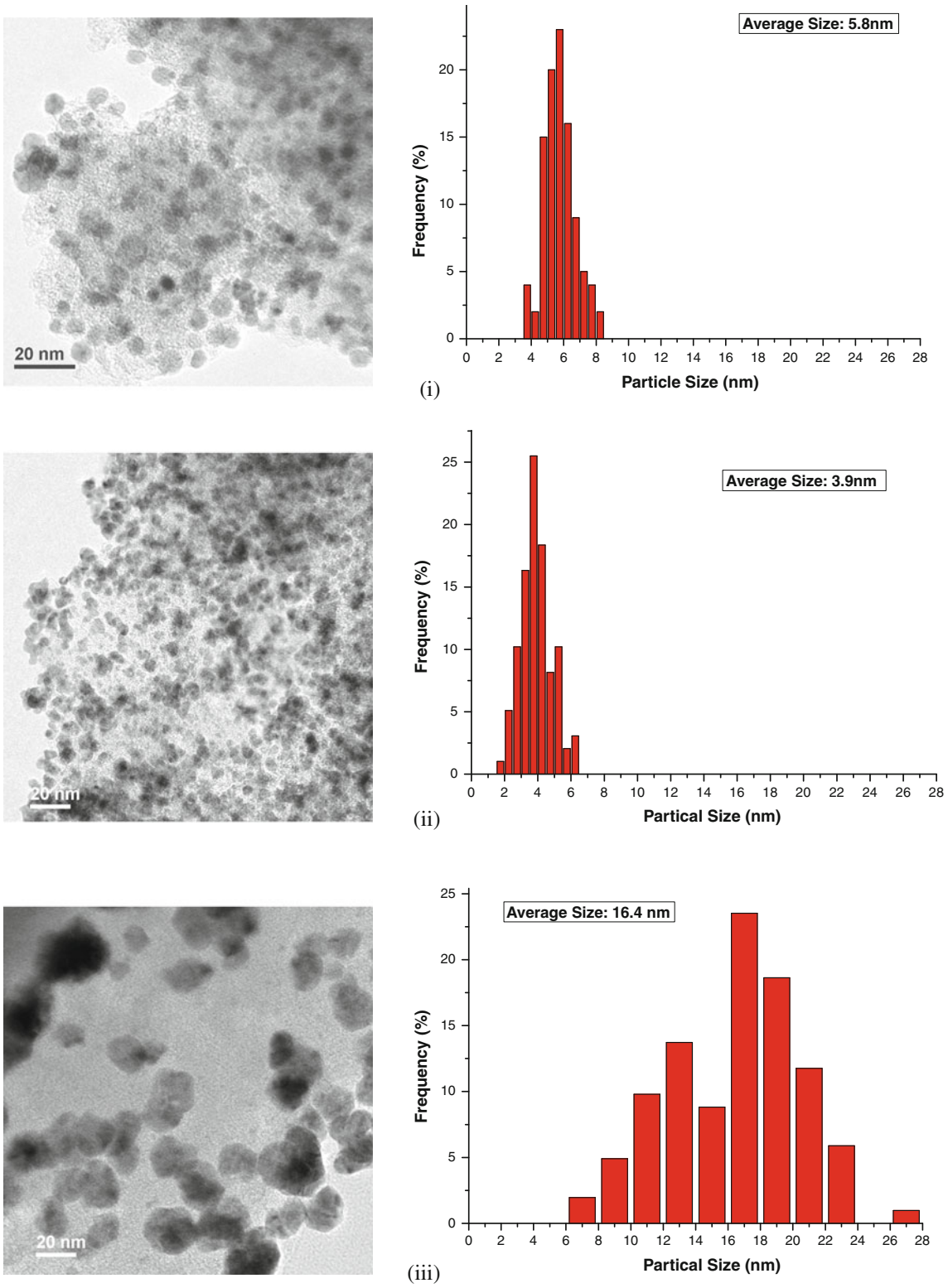

Fig. 2 Characterizations of Pd nanocrystals prepared from different precursors *i* $PdCl_2$, *ii* $Pd(OAc)_2$, *iii* $PdCl_2(en)_2$

The effect of reaction pressure at 363 K is shown in Fig. 4b (detail numbers were shown in ESI) showing that with the increase in reaction pressure, the conversion increased while the selectivity to *p*-CP was maintained. The maximum selectivity over 89 % was obtained when the system pressure was 8.0. When the reaction pressure

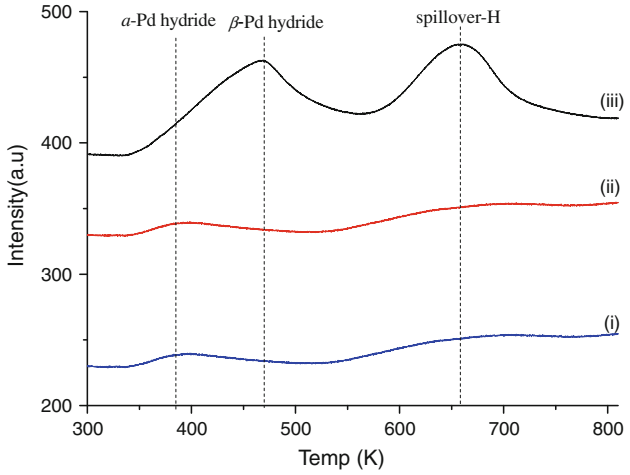

Fig. 3 TPD profiles of Pd catalysts prepared from different precursors *i* $PdCl_2(en)_2$, *ii* $PdCl_2$, *iii* $Pd(OAc)_2$

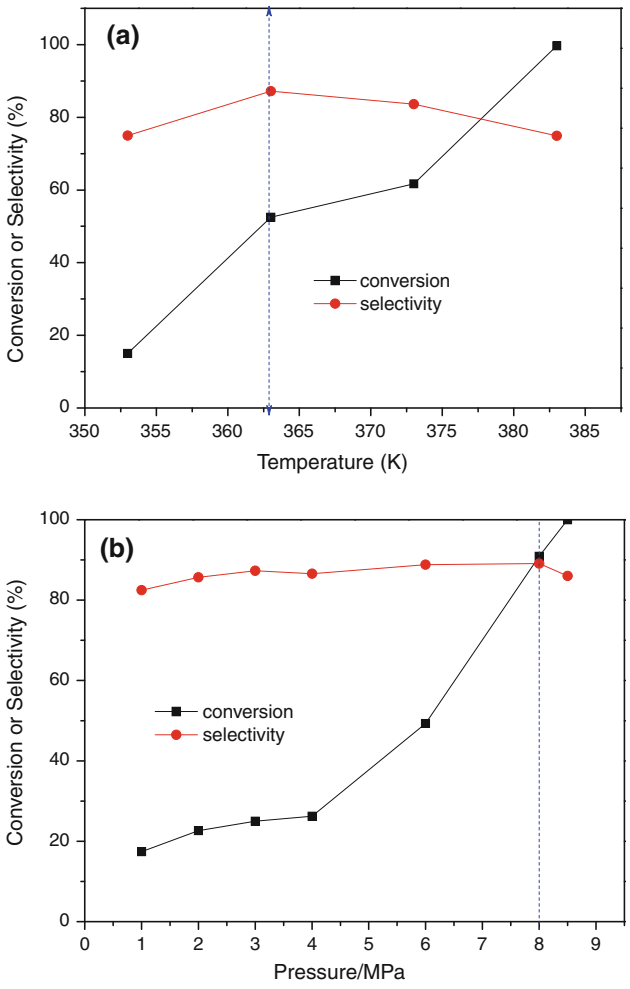

Fig. 4 Effect of temperature and pressure **a** the effect of reaction temperature (at 4.0 MPa, *p*-PP 1.5 g, THF 20 mL, cat. 0.5 g, 2 h) **b** the effect of reaction pressure (at 363 K, *p*-PP 1.5 g, THF 20 mL, cat.0.5 g, 1 h)

Table 6 Recycling conditions of Pd/AC in hydrogenation of *p*-PP

Entry	Conv. (%)	*p*-CP (%)
1	100	89.1
2	97.2	88.8
3	94.6	88.4
4	90.7	88.3

Reaction conditions: *p*-PP 1.5 g, THF 20 mL, Cat. 0.5 g, 1.5 h, 363 K, 8 MPa

was increased further, higher conversion could be obtained but the selectivity decreased. Taking selectivity into account, 8.0 MPa was therefore adopted as the system reaction pressure.

Because the recycling of catalyst is an important factor in the evaluating heterogeneous catalyst, the recycling conditions of Pd/AC in the hydrogenation of *p*-PP were studied and the results were shown in Table 6. It could be found that even after used four times, the Pd/AC can still maintain the activity (the conversion was still over 90 %) and the selectivity to *p*-CP was not changed much.

3.6 Proposed Reaction Mechanism

After detailed analysis of the product structure by GC-IR [34], the process of the reaction was monitored under the optimal conditions established above. As the reaction time progressed, the *p*-CP and *p*-PC accumulated as the main products, while the *p*-CC maintained in trace amount. The pathway of *p*-PP hydrogenation is illustrated in Scheme 2. It can be found that raw material *p*-PP is hydrogenated to *p*-CP and *p*-PC in parallel, and both *p*-CP and *p*-PC can both be further hydrogenated to the stable final product *p*-CC. Due to the hydrophobicity of the carbon support, the reaction is much more inclined to undergo path I rather than path II, which induces the high yield of *p*-CP in this catalytic system.

In order to better understand the reaction mechanism, the profile of component concentration versus reaction time is shown in Fig. 5. It is clear that *p*-PP in the reaction solution was almost completely converted into *p*-CP and *p*-PC within 1.5 h at an average dissipation rate of 2.93×10^{-1} mol/L/h. However, the increasing rate of *p*-CC in the reaction solution is only 6.67×10^{-4} mol/L/h which is 440 times slower than the rate of *p*-PP to *p*-PC and *p*-CP. In principle, this rate difference is large enough to stop the reaction at the intermediate step with the *p*-CP and *p*-PC as products with high selectivity under these controlled conditions.

Scheme 2 Pathways of *p*-PP hydrogenation

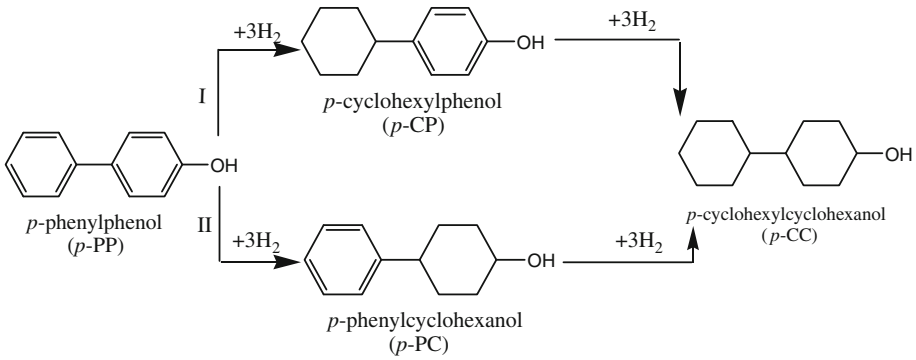

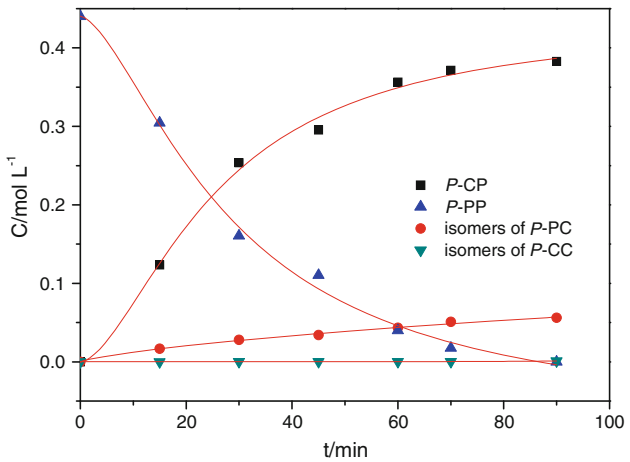

Fig. 5 Concentration–time plots for the hydrogenation of *p*-PP over Pd/AC (at 363 K, 8 MPa, Cat. 0.5 g, *p*-PP 1.5 g, THF 20mL)

4 Conclusion

A highly efficient and environmentally benign technique for the regioselective hydrogenation of *p*-PP to *p*-CP has been developed. The carbon-supported Pd nanocrystal catalyst was the most selective catalyst among those studies here. The hydrogenation of *p*-PP occurs through two parallel reaction pathways, and the *p*-CP can be produced with 89 % yield. This unique result will not only contribute to applied chemistry as a practical technique, but also promote the fundamental understanding of selective hydrogenation of other compounds containing two or more asymmetric benzene rings and their derivatives.

Acknowledgments This work was financially supported by the National High Technology Research and Development Program of China (863 Project), Grant No. 2007AA03Z345, the Scientific Research Project for Institute of Higher Education of Education Bureau, Liaoning, Grant No. LT2010021 and the Fundamental Research Funds for Dalian University of Technology DUT10RC (3)107.

References

1. Engelhard Industries (1967) GB Patent 1 068 264
2. Ungnade HE, McLaren AD (1944) J Am Chem Soc 66:118
3. Anand R, Daniel T, Lahoti RJ, Srinivasan KV, Rao BS (2002) Catal Lett 81:241
4. Postnova MV, Koshel' SG, Lebedeva NV, Kuznetsova EA, Koshel' GN (2003) Rus J Org Chem 39:1415
5. Smith HA, Alderman JDM, Shacklett CD, Welch CM (1949) J Am Chem Soc 71:3772
6. Sapre AV, Gates BC (1981) Ind Eng Chem Process Des Dev 20:68
7. Sapre AV, Gates BC (1982) Ind Eng Chem Process Des Dev 21:86
8. Lu LH, Rong ZM, Du WQ, Ma SH, Hu S (2009) Chem Cat Chem 3:369
9. Hiyoshi N, Rode CV, Sato O, Shirai M (2005) Appl Catal A-Gen 43:288
10. Tsukinoki T, Kanda T, Liu GB, Tsuzuki H, Tashiro M (2000) Tetrahedron Lett 41:5865
11. Musser DM, Adkins H (1938) J Am Chem Soc 60:664
12. Minabe M, Watanabe K, Ayabe Y (1987) J Org Chem 52:1745
13. Xin JN, Lu LH, Wang Y, Peng XJ (2008) Catal Commun 9:2345
14. Lu LH, Guo F, Xin JN (2007) CN Patent 1970143
15. Boehm HP, Diehl E, Heck W, Sappok R (1964) Angew Chem Int 3:669
16. Boehm HP (1994) Carbon 32:759
17. Boehm HP (2002) Carbon 40:145
18. Yen CH, Lin HW, Tan C-S (2011) Catal Today 174:121
19. Dillon AC, Jones KM, Bekkedahl TA, Kiang CH, Bethune DS, Heben MJ (1997) Nature 386:377
20. Liu C, Fan YY, Liu M, Cong HT, Cheng HM, Dresselhaus MS (1999) Science 286:1127
21. Velu S, Kapoor MP, Inagaki S (2003) Appl Catal A Gen 245:317
22. Neri G, Visco AM, Donato A (1994) Appl Catal A Gen 110:49
23. Mahata N, Raghavan KV, Vishwanathan V (2001) Phys Chem Chem Phys 3:2712
24. Ahnert F, Arafat HA, Pinto NG (2003) Adsorption 9:311
25. Tessier D, Rakai A, Bozon-Verduraz F (1992) Faraday Trans 88:741
26. Ali SH, Goodwin JG (1998) J Catal 176:3
27. Sepulveda J, Figoli N (1994) React Kinet Catal Lett 53:155
28. Sales EA, Bugli G, de Ensuque A, Mendes JM, Bozon-Verduraz F (1999) Phys Chem Chem Phys 1:491
29. Contescu C, Macovei D, Craiu C, Teodorescu C, Schwarz JA (1995) Langmuir 11:2031
30. Deligianni H, Mieville RL, Peri JB (1985) J Catal 95:465
31. Kelly KP, Tatsumi T, Uematsu T, Driscoll DJ, Lunsford JH (1986) J Catal 101:396
32. Bozon-Verduraz F, Omar A, Escard J, Pontvianne B (1978) J Catal 53:126
33. Amorim C, Keane MA (2008) J Colloid Interface Sci 322:196
34. Xin JN, Xu Q, Zhang H (2008) Spectrosc Spectr Anal 28:784